



Non-Oberbeck–Boussinesq zonal flow generation

Held, M.; Wiesenberger, Matthias; Kube, R.; Kendl, A.

Published in:
Nuclear Fusion

Link to article, DOI:
[10.1088/1741-4326/aad28e](https://doi.org/10.1088/1741-4326/aad28e)

Publication date:
2018

Document Version
Publisher's PDF, also known as Version of record

[Link back to DTU Orbit](#)

Citation (APA):
Held, M., Wiesenberger, M., Kube, R., & Kendl, A. (2018). Non-Oberbeck–Boussinesq zonal flow generation. *Nuclear Fusion*, 58(10), [104001]. <https://doi.org/10.1088/1741-4326/aad28e>

General rights

Copyright and moral rights for the publications made accessible in the public portal are retained by the authors and/or other copyright owners and it is a condition of accessing publications that users recognise and abide by the legal requirements associated with these rights.

- Users may download and print one copy of any publication from the public portal for the purpose of private study or research.
- You may not further distribute the material or use it for any profit-making activity or commercial gain
- You may freely distribute the URL identifying the publication in the public portal

If you believe that this document breaches copyright please contact us providing details, and we will remove access to the work immediately and investigate your claim.

LETTER • OPEN ACCESS

Non-Oberbeck–Boussinesq zonal flow generation

To cite this article: M. Held *et al* 2018 *Nucl. Fusion* **58** 104001

View the [article online](#) for updates and enhancements.

Related content

- [Zonal flows and pattern formation](#)
Ö D Gürçan and P H Diamond
- [How does drift wave turbulence convert parallel compression into perpendicular flows?](#)
Lu Wang, P H Diamond and T S Hahm
- [Isotope effect on gyro-fluid edge turbulence and zonal flows](#)
O H H Meyer and A Kendl

Letter

Non-Oberbeck–Boussinesq zonal flow generation

M. Held^{1,a} , M. Wiesenberger² , R. Kube³  and A. Kendl¹ 

¹ Institute for Ion Physics and Applied Physics, Universität Innsbruck, A-6020 Innsbruck, Austria

² Department of Physics, Technical University of Denmark, DK-2800 Kgs. Lyngby, Denmark

³ Department of Physics and Technology, UiT The Arctic University of Norway, N-9037 Tromsø, Norway

E-mail: markus.held@uibk.ac.at, mattwi@fysik.dtu.dk, ralph.kube@uit.no
and alexander.kendl@uibk.ac.at

Received 6 April 2018, revised 19 June 2018

Accepted for publication 11 July 2018

Published 26 July 2018



Abstract

Novel mechanisms for zonal flow (ZF) generation for both large relative density fluctuations and background density gradients are presented. In this non-Oberbeck–Boussinesq (NOB) regime ZFs are driven by the Favre stress, the large fluctuation extension of the Reynolds stress, and by background density gradient and radial particle flux dominated terms. Simulations of a nonlinear full-F gyro-fluid model confirm the predicted mechanism for radial ZF propagation and show the significance of the NOB ZF terms for either large relative density fluctuation levels or steep background density gradients.

Keywords: zonal flows, poloidal rotation, non-Oberbeck–Boussinesq effects, full-F gyro/drift-fluid theory, Reynolds stress, Favre stress

(Some figures may appear in colour only in the online journal)

1. Introduction

Self-organization from turbulent to coherent states is a ubiquitous process in fluids. In particular, much interest and effort has been drawn to the formation of zonal flows (ZFs) [1–3]. These coherent flows arise in atmospheres, in the form of banded cloud structures on Jupiter [4], Saturn’s north-polar hexagon [5] or mid-latitude westerlies on earth and in the ocean as stationary jets [6]. In magnetized fusion plasmas ZFs are key players for the reduction of the radial transport of particles and heat and for the transition to improved confinement regimes in tokamaks [7–12].

Reynolds stress is quintessential for ZF generation in all fluids [1–3, 13–17], but in magnetized plasmas also other stresses like the Maxwell [18, 19] or the diamagnetic stress

[20, 21] can become significant. Virtually all of the work on ZF theory so far rely on δf models [1, 13, 22], which invoke the so called Oberbeck–Boussinesq (or thin layer) approximation [23, 24]. However, the latter breaks down, if the background density varies over more than one order of magnitude or if the relative density fluctuations exceed roughly 10%. This for example prevails in the edge of tokamak fusion plasmas, where experimental measurements typically feature relative density fluctuation levels around the order 0.1 in the edge and up to unity at the last closed flux surface [25–33]. Moreover, typical edge background density gradient (e-folding) lengths reach from $50\rho_{s0}$ in low-confinement to $10\rho_{s0}$ in high-confinement tokamak plasmas [34, 35]. Here, $\rho_{s0} := \sqrt{T_{e0}m_i}/(eB_0)$ is the drift scale with reference electron temperature T_{e0} , ion particle charge e , ion mass m_i and reference magnetic field B_0 .

Non-Oberbeck–Boussinesq (NOB) effects on ZF generation are an unresolved issue. However, theoretical and experimental studies of poloidal ZFs in the edge of fusion plasmas indicate that unknown mechanisms beyond the Reynolds

^a Author to whom any correspondence should be addressed.



Original content from this work may be used under the terms of the [Creative Commons Attribution 3.0 licence](https://creativecommons.org/licenses/by/3.0/). Any further distribution of this work must maintain attribution to the author(s) and the title of the work, journal citation and DOI.

stress exist [36] and that steep background density gradients and large relative density fluctuations affect the poloidal ZF dynamics [15, 37, 38]. Moreover, the importance of large relative density fluctuations for toroidal momentum transport, as suggested by theoretical estimates in the strong and weak turbulence regime [39, 40] and experimental measurements in the TORPEX and PANTA device [41, 42], point towards a similar significance for poloidal momentum transport.

In the following we generalize the theory of ZFs to NOB effects. To this end, we decompose the density and electric potential of a full-F gyro-fluid model of a magnetized plasma [43] with the help of a density weighted Favre average [44]. This well known decomposition strategy in compressible fluid dynamics (see e.g. [45]) is here for the first time introduced to plasma physics and enables us to disentangle the density fluctuations from the ZF dynamics, while retaining the relevant physical effects. As a result, we identify novel agents in the poloidal ZF dynamics, which become significant for high relative density fluctuations or steep background density gradients. We confirm the herein proposed NOB mechanism for radial advection of ZFs with the help of numerical simulations of a fully nonlinear model for drift wave-ZF dynamics. The exploited model is based on the specified extension of the Hasegawa–Wakatani model to the full-F framework. Additionally, we show how the ZF dynamics is distributed among the proposed NOB actors and provide scalings with collisionality, reference background density gradient length and the maximum of the relative density fluctuation amplitude.

2. ZF theory

2.1. δf formalism

We start our discussion with a short re-derivation of the conventional ZF equation and Reynolds stress from a cold ion δf gyro-fluid model, which couples small relative density fluctuations to the electric potential via $\mathbf{E} \times \mathbf{B}$ advection and linear polarization [46–48]

$$\frac{\partial}{\partial t} \delta n + \nabla \cdot (\delta n \mathbf{u}_E) + \frac{1}{L_n B_0} \frac{\partial}{\partial y} \phi = \Lambda_\delta, \quad (1a)$$

$$\frac{\partial}{\partial t} \delta N + \nabla \cdot (\delta N \mathbf{u}_E) + \frac{1}{L_n B_0} \frac{\partial}{\partial y} \phi = 0, \quad (1b)$$

$$\nabla \cdot \left(\frac{1}{\Omega_0} \frac{\nabla_\perp \phi}{B_0} \right) = \delta n - \delta N. \quad (1c)$$

Here, $\delta n := n/n_G - 1$ is the relative electron density fluctuation, $\delta N := N/n_G - 1$ is the relative ion gyro-center density fluctuation, ϕ is the electric potential and $\Omega_0 := eB_0/m_i$ is the ion gyro-frequency. The reference background density $n_G(x)$ refers to a constant reference background gradient length $L_n := -1/\partial_x \ln(n_G/n_0)$ with constant reference density n_0 . For the sake of simplicity the magnetic field $B = B_0$ is assumed constant and the unit vector in the magnetic field direction is $\hat{\mathbf{b}} := \mathbf{B}/B_0 = \hat{\mathbf{e}}_z$. The perpendicular gradient and

the $\mathbf{E} \times \mathbf{B}$ drift velocity are defined by $\nabla_\perp := -\hat{\mathbf{b}} \times (\hat{\mathbf{b}} \times \nabla)$ and $\mathbf{u}_E := \hat{\mathbf{b}} \times \nabla \phi / B_0$, respectively. The term Λ_δ denotes a closure for the parallel dynamics, which is discussed later in more detail. Taking the time derivative over the polarization equation (1c) yields the δf drift-fluid vorticity density equation

$$\frac{\partial}{\partial t} \mathcal{W}_\delta + \nabla \cdot (\mathcal{W}_\delta \mathbf{u}_E) = \Omega_0 n_0 \Lambda_\delta, \quad (2)$$

with the linear $\mathbf{E} \times \mathbf{B}$ vorticity density $\mathcal{W}_\delta := n_0 \nabla_\perp^2 \phi / B_0 = \hat{\mathbf{b}} \cdot \nabla \times (n_0 \mathbf{u}_E)$. Now we apply the average over the ‘poloidal’ y coordinate $\langle h \rangle := L_y^{-1} \int_0^{L_y} dy h$ to equation (2), which is the 2D equivalent of a flux surface average. Reynolds decomposition $h = \langle h \rangle + \tilde{h}$ and integration over the ‘radial’ coordinate x result in the δf evolution equation for poloidal ZFs [13]

$$\frac{\partial}{\partial t} \langle u_y \rangle = - \frac{\partial}{\partial x} \langle \tilde{u}_x \tilde{u}_y \rangle + \Omega_0 \int_{x_0}^x dx \langle \Lambda_\delta \rangle. \quad (3)$$

Here, we introduced $u_x := -\partial_y \phi / B_0$, $u_y := \partial_x \phi / B_0$ and the anticipated Reynolds stress $\mathcal{R} := \langle \tilde{u}_x \tilde{u}_y \rangle$ [49], where $\langle u_x u_y \rangle = \langle u_x \rangle \langle u_y \rangle + \langle \tilde{u}_x \tilde{u}_y \rangle$ and $\langle u_x \rangle = 0$ was used. In passing we note that we assume that radial boundary conditions give rise to no additional terms in equation (3) and for the remainder of this letter.

2.2. Full-F formalism

In full-F theory the splitting of the gyro-fluid moment variables into fluctuating and background parts is avoided and the quasi-neutrality constraint for electrons and ions is rendered by the nonlinear polarization equation [43]. The cold ion full-F gyro-fluid model [50, 51]

$$\frac{\partial}{\partial t} n + \nabla \cdot (n \mathbf{u}_E) = \Lambda, \quad (4a)$$

$$\frac{\partial}{\partial t} N + \nabla \cdot (N \mathbf{u}_E) = 0, \quad (4b)$$

$$\nabla \cdot \left(\frac{N}{\Omega_0} \frac{\nabla_\perp \phi}{B_0} \right) = n - N, \quad (4c)$$

evolves the full electron density n and ion gyro-center density N . In the gyro-center $\mathbf{E} \times \mathbf{B}$ drift velocity by $\mathbf{U}_E := \mathbf{u}_E + \mathbf{U}_p$ the ponderomotive correction $\mathbf{U}_p := -\hat{\mathbf{b}} \times \nabla \mathbf{u}_E^2 / (2\Omega_0)$ appears. Both, the latter ponderomotive correction and the polarization charge nonlinearity on the left hand side of equation (4c) are crucial for energetic consistency and an exact momentum conservation law [52]. We refer to the parallel closure term Λ later on. In the long wavelength limit we can again reformulate equations (4b) and (4c) into a drift-fluid vorticity density equation

$$\frac{\partial}{\partial t} \mathcal{W} + \nabla \cdot (\mathcal{W} \mathbf{u}_E) - \Omega_0 \nabla \cdot (n \mathbf{U}_p) = \Omega_0 \Lambda, \quad (5)$$

where the nonlinear $\mathbf{E} \times \mathbf{B}$ vorticity density is given by $\mathcal{W} := \nabla \cdot (n \nabla_\perp \phi / B_0) = \hat{\mathbf{b}} \cdot \nabla \times (n \mathbf{u}_E)$. As above, we obtain the averaged poloidal momentum equation [38, 53, 54]

$$\begin{aligned} \frac{\partial}{\partial t} \langle nu_y \rangle = & - \frac{\partial}{\partial x} (\langle n \rangle \mathcal{R} + \langle \tilde{n} \tilde{u}_x \rangle \langle u_y \rangle + \langle \tilde{n} \tilde{u}_x \tilde{u}_y \rangle) \\ & + \Omega_0 \int_{x_0}^x dx \langle \Lambda \rangle. \end{aligned} \quad (6)$$

The divergence of the full-F stress drive terms of equation (6) is related to the averaged radial flux of vorticity density minus the ponderomotive correction via the full-F Taylor identity

$$\begin{aligned} \langle \tilde{u}_x \tilde{\mathcal{W}} \rangle = & \frac{\partial}{\partial x} (\langle n \rangle \mathcal{R} + \langle \tilde{n} \tilde{u}_x \rangle \langle u_y \rangle + \langle \tilde{n} \tilde{u}_x \tilde{u}_y \rangle) \\ & + \Omega_0 \langle \tilde{U}_{p,x} \tilde{n} \rangle. \end{aligned} \quad (7)$$

The interpretation of equation (6) is problematic since (i) absolute density fluctuations \tilde{n} arise instead of relative density fluctuations $\tilde{n}/\langle n \rangle$, (ii) the time evolution of the averaged poloidal momentum $\langle nu_y \rangle$ is given in terms of the averaged poloidal velocity $\langle u_y \rangle$ and (iii) background density gradient $\partial_x \ln \langle n \rangle$ effects are not obvious. Despite these obstacles equation (6) has been recently used to show that the second term, occasionally misinterpreted as advective, and the cubic term can be comparable to the Reynolds stress related drive $\partial_x \langle n \rangle \mathcal{R}$ [15, 37, 38].

Thus, we go a step further and utilize a density weighted Favre decomposition instead of the Reynolds decomposition according to $h := [[h]] + \hat{h}$ and $[[h]] := \langle nh \rangle / \langle n \rangle$ [44]. Note that the Favre decomposition reduces to the Reynolds decomposition if the density n is only a function of x . Now we combine the poloidal average of equation (4a) divided by $\langle n \rangle$

$$\begin{aligned} \frac{\partial}{\partial t} \ln \langle n \rangle = & - \frac{\partial}{\partial x} [[u_x]] - [[u_x]] \frac{\partial}{\partial x} \ln \langle n \rangle \\ & + \frac{\langle \Lambda \rangle}{\langle n \rangle} \end{aligned} \quad (8)$$

with equation (6) divided by $\langle n \rangle$ to obtain a ZF evolution equation for the Favre averaged poloidal velocity

$$\begin{aligned} \frac{\partial}{\partial t} [[u_y]] = & - \frac{\partial}{\partial x} [[\hat{u}_x \hat{u}_y]] - [[u_x]] \frac{\partial}{\partial x} [[u_y]] \\ & - [[\hat{u}_x \hat{u}_y]] \frac{\partial}{\partial x} \ln \langle n \rangle \\ & - [[u_y]] \frac{\langle \Lambda \rangle}{\langle n \rangle} + \frac{\Omega_0}{\langle n \rangle} \int_{x_0}^x dx \langle \Lambda \rangle, \end{aligned} \quad (9)$$

where we used $[[u_x u_y]] = [[u_x]] [[u_y]] + [[\hat{u}_x \hat{u}_y]]$. The Favre stress $\mathcal{F} := [[\hat{u}_x \hat{u}_y]]$ can be rewritten into

$$\mathcal{F} = \mathcal{R} - [[\tilde{u}_x]] [[\tilde{u}_y]] + \langle \tilde{n} \tilde{u}_x \tilde{u}_y \rangle / \langle n \rangle. \quad (10)$$

Consequently, the first term $-\partial_x \mathcal{F}$ on the right hand side of equation (9) is the superposition of the conventional Reynolds stress drive $T_1 := -\partial_x \mathcal{R}$, the quadruple fluctuation term $T_2 := \partial_x ([[\tilde{u}_x]][[\tilde{u}_y]])$ and the triple fluctuation drive $T_3 := -\partial_x (\langle \tilde{n} \tilde{u}_x \tilde{u}_y \rangle / \langle n \rangle)$. The novel second term on the right hand side of equation (9) represents radial advection of poloidal ZFs $[[u_y]]$. Its direction depends on the sign of the averaged radial particle flux $\langle \Gamma_x \rangle := \langle n \rangle [[u_x]]$, which is typically positive, so that T_4 describes an outward pinch of ZFs. The novel third term $T_5 := \mathcal{F} / L_{\langle n \rangle}$ on the right hand side of

Table 1. HW closures for δf and full-F models.

	Ordinary HW	Modified HW
$\Lambda_\delta / (\alpha_\delta \Omega_0)$	$e\phi / T_{e0} - \delta n$ [57–59]	$e\tilde{\phi} / T_{e0} - \tilde{\delta n}$ [60]
$\Lambda / (\alpha n_0 \Omega_0)$	$e\phi / T_{e0} - \ln(n / \langle n \rangle)$	$e\tilde{\phi} / T_{e0} - \ln(\tilde{n})$

equation (9) is proportional to the inverse of the background density gradient length $1/L_{\langle n \rangle} := -\partial_x \ln \langle n \rangle$. This term is large for small reference background density gradient lengths L_n , or has large radially localized values if the density profile $\langle n \rangle$ develops into a staircase like pattern [55]. In contrast to the Favre stress drive $-\partial_x \mathcal{F}$, the background density gradient drive T_5 contributes to the ZF generation even if the Favre stress is radially homogeneous $\partial_x \mathcal{F} = 0$. Remarkably, the background density gradient drive remains finite in the small relative density fluctuation limit, where the density n is only a function of x and the Favre stress \mathcal{F} resembles the conventional Reynolds stress \mathcal{R} .

In order to interpret the dynamics of the background density gradient drive T_5 let us assume for a moment that the turbulent viscosity hypothesis $\mathcal{F} := -\nu_T(x) \partial_x [[u_y]]$ holds [13, 56]. In this case equation (9) reduces to a simple advection-diffusion equation for ZFs

$$\begin{aligned} \frac{\partial}{\partial t} [[u_y]] = & - ([[u_x]] + V) \frac{\partial}{\partial x} [[u_y]] \\ & + \frac{\partial}{\partial x} \left(\nu_T \frac{\partial}{\partial x} [[u_y]] \right) - [[u_y]] \frac{\langle \Lambda \rangle}{\langle n \rangle} \\ & + \frac{\Omega_0}{\langle n \rangle} \int_{x_0}^x dx \langle \Lambda \rangle, \end{aligned} \quad (11)$$

where the background density gradient pinch velocity $V := \nu_T / L_{\langle n \rangle}$ appears now in addition to the radial outward pinch velocity $[[u_x]]$. The direction of the additional pinch depends on the sign of the turbulent viscosity ν_T .

Finally, we extend the theory for energy transfer inside the kinetic $\mathbf{E} \times \mathbf{B}$ energy $E(t) := m_i \int dA \langle n \mathbf{u}_E^2 \rangle / 2$ to the full-F formalism. Here, the Favre decomposition $E = E_0 + E_1$ is pivotal to derive the conservation laws for the zonal (or mean) $E_0(t) := m_i \int dA \langle n \rangle [[u_y]]^2 / 2$ and turbulent part $E_1(t) := m_i \int dA \langle n \rangle \hat{\mathbf{u}}_E^2 / 2$ of the kinetic $\mathbf{E} \times \mathbf{B}$ energy and supersedes the Reynolds decomposition in the δf formalism [19, 21]. With the help of equations (8) and (9) we obtain the conservation laws for the zonal and turbulent kinetic $\mathbf{E} \times \mathbf{B}$ energy

$$\begin{aligned} \frac{\partial}{\partial t} E_0 = & \int dA m_i \left(\langle n \rangle \mathcal{F} \frac{\partial}{\partial x} [[u_y]] - \frac{[[u_y]]^2}{2} \langle \Lambda \rangle \right) \\ & + \Omega_0 [[u_y]] \int_{x_0}^x dx \langle \Lambda \rangle, \end{aligned} \quad (12a)$$

$$\begin{aligned} \frac{\partial}{\partial t} E_1 = & \int dA m_i \left(-\langle n \rangle \mathcal{F} \frac{\partial}{\partial x} [[u_y]] + \frac{[[u_y]]^2}{2} \langle \Lambda \rangle \right) \\ & - \Omega_0 [[u_y]] \int_{x_0}^x dx \langle \Lambda \rangle - \frac{e}{m_i} \langle \phi \Lambda \rangle. \end{aligned} \quad (12b)$$

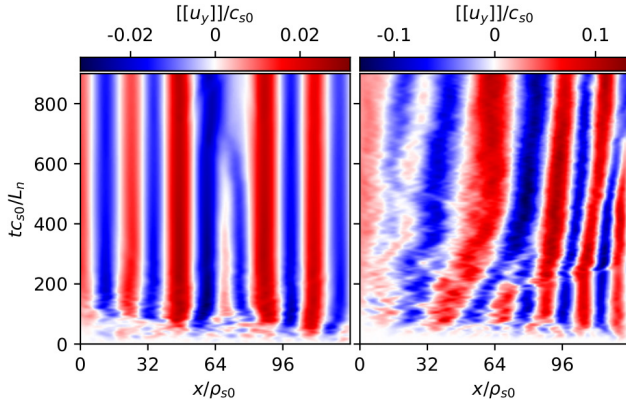


Figure 1. The spatio-temporal ZF evolution of the Favre averaged poloidal velocity $[[u_y]]$ is shown for two different reference density gradient lengths $L_n = \{128, 32\} \rho_{s0}$ (left, right) in the high collisionality regime ($\alpha = 0.0005$). Radial outward ZF advection occurs in the steep gradient regime (right).

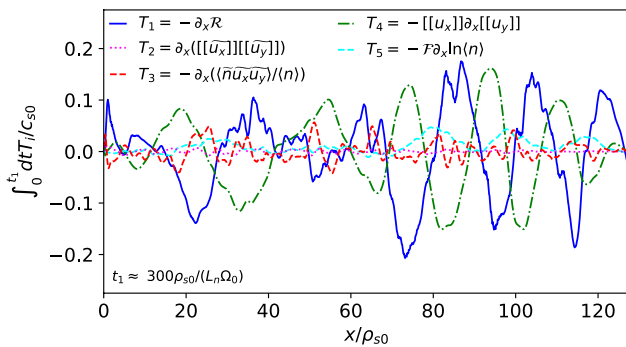


Figure 2. The radial profile of the terms of the right hand side of equation (9) for $\alpha = 0.0005$ and $L_n = 32 \rho_{s0}$. The ZF signature of the radial advection term T_4 is comparable to the Reynolds stress T_1 .

This unveils that the Favre stress term $\langle n \rangle \mathcal{F} \partial_x [[u_y]]$ is the central mechanism for energy transfer between the zonal and turbulent kinetic $\mathbf{E} \times \mathbf{B}$ energy. As a consequence, density fluctuations (see equation (10)) manifest as an additional transfer channel in the full-F formalism.

3. Parallel closures

Self-sustained drift wave turbulence is maintained by the non-adiabatic parallel coupling of the relative density fluctuations and the electric potential, which can arise due to various mechanisms. Here, we exemplarily consider resistive drift wave turbulence, which arises due to resistive friction between electrons and ions along the magnetic field line. This mechanism enters the 2D gyro-fluid models via the parallel closure terms (Λ_δ or Λ) of the Hasegawa–Wakatani (HW) type as summarized in table 1. Here, we introduced the full-F adiabaticity parameter $\alpha := T_e k_\parallel^2 / (\eta_\parallel e^2 n_0 \Omega_0)$ with parallel wavenumber k_\parallel and parallel Spitzer resistivity $\eta_\parallel := 0.51 m_e \nu_e / (n e^2)$ [61, 62]. In the electron collision frequency ν_e the Coulomb logarithm is treated as a constant so that η_\parallel has no explicit dependence on n . As opposed to this in δf models the density dependence in the collision frequency $\nu_e(n) \approx \nu_{e0}$ is completely neglected so

that $\alpha_\delta := T_e k_\parallel^2 / (0.51 m_e \nu_{e0} \Omega_0)$ reduces to a parameter. Only then, the poloidal variations of the adiabaticity parameters vanish ($\tilde{\alpha}_\delta = \tilde{\alpha} = 0$), and the full-F and δf closures coincide in the limit of $\langle n \rangle \approx n_G$ and $\delta n \ll 1$.

4. Simulations

We use the open source library FELTOR [63] to numerically solve the full-F gyro-fluid equations (4a)–(4c) with the modified HW parallel closure of table 1. Numerical stability is ensured by adding hyperdiffusive terms of second order $-\nu \nabla_\perp^4 n$ and $-\nu \nabla_\perp^4 N$ to the right hand side of equations (4a) and (4b). Moreover, we append the right hand side of equations (4a) and (4b) by a density source of the form $\omega_S z \Theta(z)$ with $z := g(x) (n_G - \langle n \rangle)$ to maintain the initial profile in a small region $x \in [0, x_b]$. Here, we defined the Heaviside function $\Theta(z)$ and $g(x) := [1 - \tanh(x - x_b) / \sigma_b] / 2$. The corresponding parameters are fixed to $\nu = 5 \times 10^{-4} c_{s0} \rho_{s0}^3$, $\omega_S = 0.1 \Omega_0$, $x_b = 0.1 L_x$ and $\sigma_b = 0.5 \rho_{s0}$ with cold ion sound speed $c_{s0} := \rho_{s0} \Omega_0$. The box with size $L_x = L_y = 128 \rho_{s0}$ is resolved by a discontinuous Galerkin discretization with $P = 3$ polynomial coefficients and at least $N_x = N_y = 256$ equidistant grid cells. The initial (gyro-center) density fields $n(\mathbf{x}, 0) = N(\mathbf{x}, 0) = n_G(x) (1 + \delta n_0(\mathbf{x}))$ consist of the reference background density profile n_G , which is perturbed by a turbulent bath $\delta n_0(\mathbf{x})$.

NOB effects on drift wave-ZF dynamics, as it is described by equations (8) and (9) with $\langle \Lambda \rangle = 0$, are in this setup studied by varying the adiabaticity parameter (or inverse collisionality) α and the reference background gradient length L_n . In figure 1 we show that L_n crucially determines the time evolution of ZFs in the high collisionality regime with $\alpha = 0.0005$. While stationary ZFs emerge for $L_n = 128 \rho_{s0}$, a radial outward pinch of ZFs occurs for a four times smaller reference background density gradient length $L_n = 32 \rho_{s0}$.

In this steep gradient and high collisionality regime the ZF signature is no longer solely determined by the conventional Reynolds stress drive, which is illustrated in figure 2. The Reynolds stress drive T_1 is here comparable to the radial advection term T_4 , which explains the observed radial outward propagation of ZFs in figure 1.

In the following the parametric dependence of each term T_i on the right hand side of equation (9) is investigated. To this end, the contribution of each term T_i on ZF evolution is measured by taking the L^2 norm, denoted by $\|h\|_2$, of the time integrated contribution. Following this, we propose a measure of the relative ZF contribution

$$M_i := \frac{\| \int_0^{t_1} dt T_i \|_2}{\sum_{j=1}^5 \| \int_0^{t_1} dt T_j \|_2}. \quad (13)$$

In figure 3(a) we show that the relative contribution M_i of the NOB ZF terms (T_2, \dots, T_5) decreases with the reference background density gradient length L_n in the high collisionality regime ($\alpha = 0.0005$). The summed up relative contribution of the NOB ZF terms exceeds the one of the

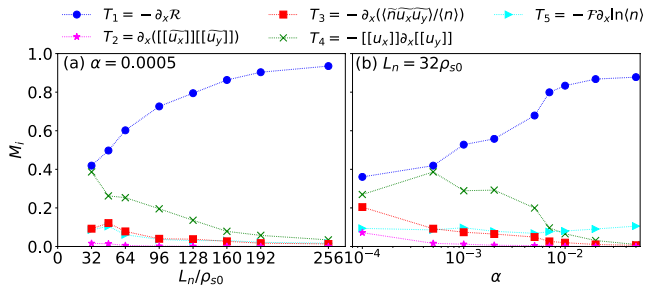


Figure 3. (a) The NOB ZF terms decrease with the reference background gradient length L_n in the high collisionality regime ($\alpha = 0.0005$). (b) For a fixed $L_n = 32\rho_{s0}$ all the NOB ZF terms significantly contribute to the ZF dynamics in the high collisionality regime. As opposed to this, only the background density gradient drive T_5 remains alongside the Reynolds stress drive T_1 in the small collisionality regime.

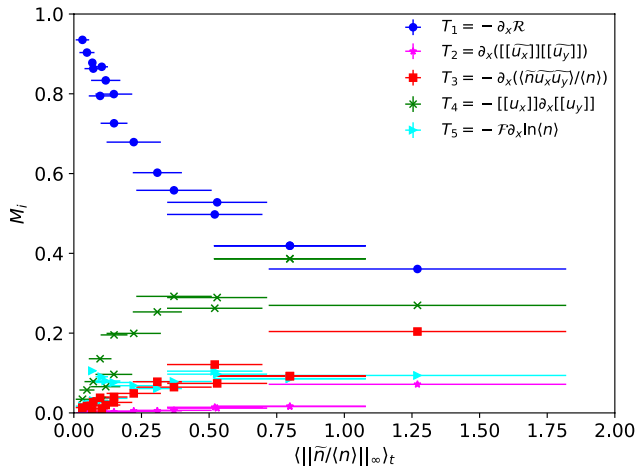


Figure 4. The relative contributions of the NOB ZF terms increase with the relative density fluctuation amplitude. In particular they can amount to roughly two thirds of the ZF dynamics.

conventional Reynolds stress for $L_n = 32\rho_{s0}$. For steep reference background density gradients the radial advection term T_4 exhibits the largest relative contribution to the ZF dynamics of all the NOB terms.

In figure 3(b) the dependence of the relative importance of each term on the adiabaticity parameter α is depicted for a fixed reference background density gradient length $L_n = 32\rho_{s0}$. While the conventional Reynolds stress term is again the dominating ZF contributor in particular for small collisionalities, all the NOB terms, except the background density gradient drive T_5 , gain in importance for higher collisionalities. Interestingly, in the small collisionality regime ($\alpha \geq 0.01$) the background density gradient drive T_5 exceeds all the remaining NOB actors. The quadruple fluctuation drive T_2 is for all studied parameters the smallest contributor to the ZF dynamics.

The dependence of the ZF terms on the time averaged maximum of the relative density fluctuation level $\langle \|\tilde{n}/\langle n \rangle\|_\infty \rangle_t$ is shown in figure 4. Here, we denote the time average by $\langle \cdot \rangle_t$ and compute the maximum with the help of the supremum

norm $\|\cdot\|_\infty$. In figure 4 the conventional Reynolds stress drive T_1 contribution weakens with increasing relative density fluctuation level. The radial advection term T_4 and the triple fluctuation drive T_3 are the dominating NOB ZF contributors for high relative density fluctuations, while the background density gradient drive T_5 can be relevant likewise for small relative density fluctuations.

5. Conclusion

We have generalized the ZF equation (3) to account for NOB effects in equation (9). Most importantly, the former Reynolds stress \mathcal{R} is replaced by the Favre stress \mathcal{F} , which adds to its predecessor in case of high relative density fluctuations. The latter is accompanied by two new agents in the NOB ZF equation (9). The first of these radially advects ZFs by the Favre averaged radial drift velocity, which is proportional to the averaged radial particle flux. The second term scales inversely with the background density gradient length and affects the ZF dynamics even if the relative density fluctuations are small or if the Favre stress is radially homogeneous. Thus, this term may be of significance in or during the formation of radial transport barriers, where steep density profiles form with strongly reduced radial particle transport.

Additionally we extended the ordinary and modified HW model to the full-F theory. We simulated the full-F gyro-fluid model with the modified HW closure to numerically corroborate our theoretical results. The simulations successfully reproduced the predicted radial advection of ZFs, which appeared for small reference background density gradient lengths and large averaged radial particle flux. Moreover, our numerical parameter study showed that the NOB ZF drives can be comparable to the Reynolds stress drive in the herein scanned parameter range. In particular the deviation between the Reynolds and Favre stress drive increases with the relative density fluctuation amplitude, collisionality and inversely with the reference background density gradient length. This deviation is mainly reasoned in the triple fluctuation drive. Its importance in steep background density gradient regimes is in qualitative agreement with the theoretical estimate in the strong turbulence regime [38]. A similar dependence as for the Favre stress drive is found for the radial ZF advection mechanism. For the background density gradient drive only a dependence on the reference background density gradient is observed.

The presented results strongly argue in favor of the development and application of full-F gyro-fluid or gyro-kinetic models for simulation of fusion edge plasma turbulence, and in general demonstrate exemplarily the relevance of NOB effects for ZF formation in fluids and plasmas with large fluctuations and inhomogeneities. The latter conditions prevail e.g. during the low- to high-confinement mode transition. Thus, a consistent full-F simulation approach of this phenomenon is crucial to allow for the herein presented NOB ZF mechanisms.

Finally, we emphasize that the relative error between the Favre and Reynolds average of the poloidal velocity, derived to $|\langle \tilde{u}_y \rangle| / \langle u_y \rangle$, is typically below a few percent. Thus, our proposed NOB ZF theory is also applicable to experimental measurements of the Reynolds averaged poloidal velocity $\langle u_y \rangle$.

Acknowledgments

This work was supported by the Austrian Science Fund (FWF) Y398. R.K. was supported with financial subvention from the Research Council of Norway under grant 240510/F20. The computational results presented have been achieved using the Vienna Scientific Cluster (VSC) and the EUROfusion High Performance Computer (Marconi-Fusion). This work has been carried out within the framework of the EUROfusion Consortium and has received funding from the Euratom research and training programme 2014–2018 under grant agreement No 633053. The views and opinions expressed herein do not necessarily reflect those of the European Commission.

ORCID iDs

M. Held  <https://orcid.org/0000-0001-8171-8038>
 M. Wiesenberger  <https://orcid.org/0000-0002-5921-0163>
 R. Kube  <https://orcid.org/0000-0003-1635-6151>
 A. Kendl  <https://orcid.org/0000-0002-4270-9160>

References

- [1] Diamond P.H., Itoh S.I., Itoh K. and Hahn T.S. 2005 *Plasma Phys. Control. Fusion* **47** R35
- [2] Fujisawa A. 2009 *Nucl. Fusion* **49** 013001
- [3] Gürçan Ö.D. and Diamond P.H. 2015 *J. Phys. A: Math. Theor.* **48** 293001
- [4] Heimpel M., Aurnou J. and Wicht J. 2005 *Nature* **438** 193–6
- [5] Baines K.H., Momary T.W., Fletcher L.N., Showman A.P., Roos-Serote M., Brown R.H., Buratti B.J., Clark R.N. and Nicholson P.D. 2009 *Planet. Space Sci.* **57** 1671–81
- [6] Maximenko N.A., Bang B. and Sasaki H. 2005 *Geophys. Res. Lett.* **32** L12607
- [7] Burrell K.H. 1997 *Phys. Plasmas* **4** 1499–518
- [8] Terry P.W. 2000 *Rev. Mod. Phys.* **72** 109–65
- [9] Hillesheim J.C., Delabie E., Meyer H., Maggi C.F., Meneses L., Poli E. and JET Contributors (EUROfusion Consortium, JET, Culham Science Centre, Abingdon, Oxon OX14 3DB, United Kingdom) 2016 *Phys. Rev. Lett.* **116** 065002
- [10] Tynan G.R., Cziegler I., Diamond P.H., Malkov M., Hubbard A., Hughes J.W., Terry J.L. and Irby J.H. 2016 *Plasma Phys. Control. Fusion* **58** 044003
- [11] Schmitz L. 2017 *Nucl. Fusion* **57** 025003
- [12] Cziegler I., Hubbard A.E., Hughes J.W., Terry J.L. and Tynan G.R. 2017 *Phys. Rev. Lett.* **118** 105003
- [13] Diamond P.H. and Kim Y. 1991 *Phys. Fluids B: Plasma Phys.* **3** 1626–33
- [14] Xu Y.H., Yu C.X., Luo J.R., Mao J.S., Liu B.H., Li J.G., Wan B.N. and Wan Y.X. 2000 *Phys. Rev. Lett.* **84** 3867–70
- [15] Müller H. et al (The ASDEX Upgrade Team) 2011 *Nucl. Fusion* **51** 073023
- [16] Xu G.S. et al 2011 *Phys. Rev. Lett.* **107** 125001
- [17] Yan Z., McKee G.R., Fonck R., Gohil P., Groebner R.J. and Osborne T.H. 2014 *Phys. Rev. Lett.* **112** 125002
- [18] Craddock G.G. and Diamond P.H. 1991 *Phys. Rev. Lett.* **67** 1535–8
- [19] Scott B.D. 2005 *New J. Phys.* **7** 92
- [20] Smolyakov A.I., Diamond P.H. and Medvedev M.V. 2000 *Phys. Plasmas* **7** 3987–92
- [21] Madsen J., Rasmussen J.J., Naulin V. and Nielsen A.H. 2017 *Phys. Plasmas* **24** 062309
- [22] Guo Z.B. and Diamond P.H. 2016 *Phys. Rev. Lett.* **117** 125002
- [23] Oberbeck A. 1879 *Ann. Phys. Chem.* **7** 271
- [24] Boussinesq J. 1903 *Theorie Analytique De La Chaleur* vol 2 (Paris: Gauthier-Villars)
- [25] Surko C.M. and Slusher R.E. 1983 *Science* **221** 817–22
- [26] Liewer P.C. 1985 *Nucl. Fusion* **25** 543
- [27] Ritz C., Brower D., Rhodes T., Bengtson R., Levinson S., Levinson N. Jr, Peebles W. and Powers E. 1987 *Nucl. Fusion* **27** 1125
- [28] Fonck R.J., Cosby G., Durst R.D., Paul S.F., Bretz N., Scott S., Synakowski E. and Taylor G. 1993 *Phys. Rev. Lett.* **70** 3736–9
- [29] Endler M., Niedermeyer H., Giannone L., Kolzhauer E., Rudyj A., Theimer G. and Tsois N. 1995 *Nucl. Fusion* **35** 1307
- [30] McKee G. et al 2001 *Nucl. Fusion* **41** 1235
- [31] Zweben S.J., Boedo J.A., Grulke O., Hidalgo C., LaBombard B., Maqueda R.J., Scarin P. and Terry J.L. 2007 *Plasma Phys. Control. Fusion* **49** S1
- [32] Zweben S. et al (The NSTX Team) 2015 *Nucl. Fusion* **55** 093035
- [33] Gao X., Zhang T., Han X., Zhang S., Kong D., Qu H., Wang Y., Wen F., Liu Z. and Huang C. 2015 *Nucl. Fusion* **55** 083015
- [34] Shao L.M., Wolfrum E., Ryter F., Birkenmeier G., Laggner F.M., Viezzer E., Fischer R., Willensdorfer M., Kurzan B., Lunt T. and The ASDEX Upgrade Team 2016 *Plasma Phys. Control. Fusion* **58** 025004
- [35] Kobayashi T. et al 2016 *Sci. Rep.* **6** 30720
- [36] Kobayashi T. et al 2013 *Phys. Rev. Lett.* **111** 035002
- [37] Windisch T., Grulke O., Naulin V. and Klinger T. 2011 *Plasma Phys. Control. Fusion* **53** 124036
- [38] Wang L., Wen T. and Diamond P. 2016 *Nucl. Fusion* **56** 106017
- [39] Wang L., Wen T. and Diamond P.H. 2015 *Phys. Plasmas* **22** 052302
- [40] Kosuga Y., Itoh S.I., Diamond P.H. and Itoh K. 2017 *Phys. Rev. E* **95** 031203
- [41] Labit B., Theiler C., Fasoli A., Furno I. and Ricci P. 2011 *Phys. Plasmas* **18** 032308
- [42] Inagaki S. et al 2016 *Sci. Rep.* **6** 22189
- [43] Madsen J. 2013 *Phys. Plasmas* **20** 072301
- [44] Favre A. 1965 *J. Mec.* **4** 361–90
- [45] Wilcox D.C. 2000 *Turbulence Modeling for CFD* (La Cañada Flintridge, CA: DCW Industries)
- [46] Dorland W. and Hammett G.W. 1993 *Phys. Fluids B* **5** 812
- [47] Beer M.A. and Hammett G.W. 1996 *Phys. Plasmas* **3** 4046
- [48] Scott B. 2010 *Phys. Plasmas* **17** 102306
- [49] Reynolds O. 1895 *Phil. Trans. R. Soc. A* **186** 123–64
- [50] Wiesenberger M., Madsen J. and Kendl A. 2014 *Phys. Plasmas* **21** 092301
- [51] Held M., Wiesenberger M., Madsen J. and Kendl A. 2016 *Nucl. Fusion* **56** 126005
- [52] Scott B. and Smirnov J. 2010 *Phys. Plasmas* **17** 112302

- [53] Gürçan Ö.D., Diamond P.H., Hahn T.S. and Singh R. 2007 *Phys. Plasmas* **14** 042306
- [54] Shurygin R.V. 2012 *Plasma Phys. Rep.* **38** 93–9
- [55] Dif-Pradalier G. et al 2015 *Phys. Rev. Lett.* **114** 085004
- [56] Pope S.B. 2000 *Turbulent Flows* (Cambridge: Cambridge University Press)
- [57] Hasegawa A. and Wakatani M. 1983 *Phys. Rev. Lett.* **50** 682
- [58] Wakatani M. and Hasegawa A. 1984 *Phys. Fluids* **27** 611
- [59] Hasegawa A. and Wakatani M. 1987 *Phys. Rev. Lett.* **59** 1581–4
- [60] Numata R., Ball R. and Dewar R.L. 2007 *Phys. Plasmas* **14** 102312
- [61] Spitzer L. 1956 *Physics of Fully Ionized Gases* (New York: Interscience)
- [62] Lingam M., Hirvijoki E., Pfefferlé D., Comisso L. and Bhattacharjee A. 2017 *Phys. Plasmas* **24** 042120
- [63] Wiesenberger M. and Held M. 2018 FELTOR v4.0 (<https://doi.org/10.5281/zenodo.1167635>)